Photoelectrochemical characteristics of TiO_2 nanorod arrays grown on fluorine doped tin oxide substrates by the facile seeding layer assisted hydrothermal method*

SUI Mei-rong (隋美蓉)[1]**, **HAN Cui-ping** (韩翠平)[1], **GU Xiu-quan** (顾修全)[2], **WANG Yong** (王永)[1], **TANG Lu** (唐璐)[1], **and TANG Hui** (唐慧)[1]

1. School of Medical Imaging, Xuzhou Medical College, Xuzhou 221004, China

2. School of Materials Science and Engineering, China University of Mining and Technology, Xuzhou 221116, China

(Received 4 November 2015; Revised 4 February 2016)

TiO_2 nanorod arrays (NRAs) were prepared on fluorine doped tin oxide (FTO) substrates by a facile two-step hydrothermal method. The nanorods were selectively grown on the FTO regions which were covered with TiO_2 seeding layer. It took 5 h to obtain the compact arrays with the nanorod length of ~2 μm and diameter of ~50 nm. The photoelectrochemical (PEC) properties of TiO_2 NRAs are also investigated. It is demonstrated that the TiO_2 NRAs indicate the good photoelectric conversion ability with an efficiency of 0.22% at a full-wavelength irradiation. A photocurrent density of 0.21 mA/cm^2 is observed at 0.7 V versus the saturated calomel electrode (SCE). More evidences suggest that the charge transferring resistance is lowered at an irradiation, while the flat-band potential (V_{fb}) is shifted towards the positive side.

Document code: A **Article ID:** 1673-1905(2016)03-0161-5

DOI 10.1007/s11801-016-5242-z

As a common photocatalyst, TiO_2 can be easily formed to thin nanoparticles (NPs, less than 20 nm) which can be assembled into the mesoporous films with high surface areas and continuous porous structures. Up to now, there have been lots of reports on the applications of mesoporous TiO_2 films in the fields, including solar water splitting[1,2] and solar cells[3]. Nevertheless, mesoporous TiO_2 films encounter the slow charge transport rate and the resulting short diffusion distance. One-dimensional (1D) arrayed structures might be good alternatives, of which the carrier transport is ~100 times rapider than that of mesoporous films[4,5]. Compared with metallic Ti foils, the transparent conducting substrates seem more advantageous for the growth of aligned TiO_2 nanorod arrays (NRAs). As a transparent conductive oxide (TCO), the fluorine-doped tin oxide (FTO, SnO_2:F) is commonly used as a substrate for growing TiO_2 NRAs due to its small lattice mismatch (just 2%) with rutile TiO_2. Up to now, there have been a number of reports on the preparation and application of TiO_2 NRAs on FTO[6-8]. For instance, Berhe et al[6] realized the growth of very thin (~20 nm) single-crystalline rutile TiO_2 nanorod films on FTO substrates through a seeding layer assisted hydrothermal method, and investigated the influence of seeding and bath conditions on the nanorod growth. Qin et al[7] reported a simple hydrothermal method for preparing highly oriented and crystalline anatase TiO_2 NRAs, which were advantageous as photoanodes for water photoelectrolysis. Additionally, Lv et al[8] recently developed a modified hydrothermal method for synthesizing TiO_2 NRAs with a loose structure and an average length of ~30 μm, which resulted in the record efficiency of ~7.91% for power conversion when they were used as the dye-sensitized solar cell (DSSC) photoanodes.

In consideration of the larger scale application, it is necessary to set aside a bare TCO region for connecting to the wires or probes before the DSSC assembly. However, if a common hydrothermal or solvothermal method is used, the whole FTO surface might be covered with TiO_2 NRAs completely due to the seeding role of SnO_2 grains from FTO layers. Thus, it is necessary to develop new methods for realizing a selective area growth of TiO_2 NRAs on FTO to avoid the post-growth treatments, such as the scratching of sandpapers. In this paper, we synthesized TiO_2 NRAs with a two-stage hydrothermal method. In detail, the FTO glass is coated with a layer of TiO_2 NPs before the growth of the arrays. Such a thin layer can efficiently enhance the performance of TiO_2 NRA based perovskite solar cells[9]. However, there were very few reports on the effect of thin seeding layers on the morphology and photoelectrochemical (PEC) performance of TiO_2 NRAs. In term of our studies, it is

* This work has been supported by the Science and Technology Projects of Xuzhou City (No.KC14SM088), and the Natural Science Fund for Colleges and Universities in Jiangsu Province (No.15KJB430031).

** E-mail: smr2012@xzmc.edu.cn

found that thin TiO_2 NPs actually play a role of seeding, which is in favor of the rapid growth of nanorods. Moreover, the PEC performance of TiO_2 NRAs is evaluated by a 3-electrode cell connected with an electrochemical workstation. The mechanism is revealed by the electrochemical impedance techniques.

All chemical reagents used in this work, including the tetrabutyl titanate ($C_{16}H_{36}O_4Ti$), titanium tetrachloride ($TiCl_4$), hydrochloric acid (37% HCl) and ethanol, are all analytical grade without further purification or other treatments. And all the aqueous solutions were prepared using deionized (DI) water. Prior to use, the FTO coated glass slices with thickness of 2 mm, which were used as substrates, were ultrasonic cleaned by acetone, ethanol and DI water, respectively.

Firstly, a 2 mol/L $TiCl_4$ aqueous solution was prepared through dipping the $TiCl_4$ (22 mL) precursor into the ice (78 mL), with stirring continuously. Then, the $TiCl_4$ aqueous solution was diluted to a concentration of 60 mmol/L by putting 1.5 mL thick $TiCl_4$ solution into 49 mL water.

TiO_2 NRAs were prepared on FTO coated glass substrates by a facile two-stage, seeding layer assisted hydrothermal method. At first, the cleaned FTO slices were partly covered with adhesive tape which could endure a relatively high temperature (~400 °C), in order to prevent the growth of NRAs in the certain region. Then, the FTO substrates were laid in a baker filled with diluted $TiCl_4$ solution (60 mmol/L) at 70 °C for 1 h. Afterwards, those glass slices were placed in a sealed autoclave (with volume of 100 mL) with the conductive side facing down. A precursor solution, containing 0.6 mL tetrabutyl titanate, 15 mL hydrochloric acid (with weight percent of 37%) and 15 mL DI water, was then poured into the autoclave.

After the hydrothermal reaction for another 5 h at 170 °C, the slides were taken out and then washed with DI water and ethanol in turn for several times. Finally, the samples were dried at 80 °C for 12 h in a vacuum oven overnight, followed by a 500 °C in air for 1 h to enhance the adhesion of crystalline TiO_2 NRAs on substrates.

X-ray diffraction (XRD) was carried out to characterize the phase structure of the TiO_2 samples by a D8 Advance Bruker diffractometer with Cu Kα irradiation. The surface morphologies were examined by a field emission scanning electron microscopy (FESEM, S-4800, Hitachi, Japan).

The PEC properties of the samples were evaluated by an electrochemical workstation connected with a three-electrode configuration under a simulated solar irradiation, which was provided by a 500 W Xe lamp with irradiation intensity ~100 mW/cm^2 (made in Beijing Trusttech Technology Co. Ltd.) without using the filter. As a result, a full-wavelength irradiation was output so that the TiO_2 electrodes were activated. The distance between the lamp and the solution was ~3 cm. PEC measurements were carried out with the as-prepared sample as a working electrode (typical efficient area of 1 cm^2), the Pt foil as a counter electrode (3 cm^2), and the saturated calomel electrode (SCE) as a reference electrode. A 0.1 mol/L phosphate buffer saline (PBS) solution (pH=7) was used as the electrolyte and sacrificial reagent. The current density versus potential (*J-V*) curve of the working electrode was obtained by the linear sweep voltammogram (LSV) with a potentiostat (CHI660D, CH Instruments) at a scan rate of 50 mV·s^{-1}. The photocurrent response was obtained by potentiostatic measurements (current versus time, *I-t*) under intermittent illumination at a bias of 0.0 V versus SCE. Electrochemical impedance spectroscopy (EIS) was conducted using CHI660D with an alternating current signal (10 mV) in the frequency range of 0.1—10^5 Hz at 0.0 V versus SCE. The Mott-Schottky (M-S) plots were measured at a frequency of 1 kHz in dark and under irradiation. All the measurements under irradiation were performed with backside illumination.

Fig.1 shows the typical surface and cross-sectional morphologies of TiO_2 NRAs grown on FTO substrates using the seeding layer assisted method. As we expected, the nanorods prefer to grow on the regions which were covered with thin TiO_2 layers. It assures the selective growth of TiO_2 NRAs in the certain regions. Besides, it is found that the NRAs exhibit a relatively compact structure with average nanorod length of ~2 μm and diameter of ~50 nm. Note that the whole reaction duration is 5 h, which is much shorter than those grown via traditional hydrothermal methods.

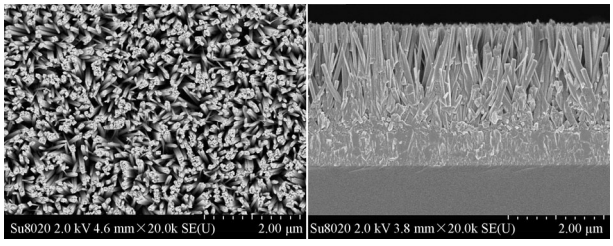

(a) (b)

Fig.1 (a) Top-view and (b) cross-sectional images of TiO_2 NRAs grown on FTO substrates directly by a facile two-stage seeding layer assisted hydrothermal method

Furthermore, the crystal structure and phase composition of the as-prepared TiO_2 NRAs were examined by XRD as illustrated in Fig.2. It is clearly observed that all the diffraction peaks can be indexed to the rutile TiO_2 (JCPDS No.42-1276) and rutile SnO_2 (JCPDS No.41-1445). Besides, only (101), (002) and (220) diffraction peaks of TiO_2 appear in the pattern, which suggests that there is a preferred orientation of NRAs. Not any peak related to anatase TiO_2 NPs is found, which might be associated with its low content. In other words, the seeding layer might be too thin to be detected.

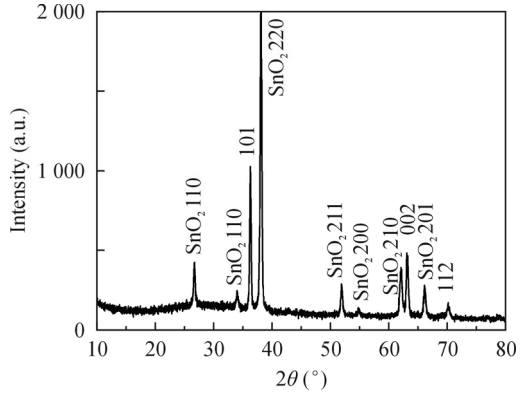

Fig.2 Typical XRD pattern of TiO_2 NRAs grown directly on FTO substrates

Fig.3 shows a typical optical absorption spectrum of TiO_2 NRA membranes. There isn't obvious absorption in the visible range, while a steep absorbance edge appears around 400 nm. It means that the TiO_2 NRAs have a good response for the photons with wavelength less than 400 nm. Further, by fitting the $(\alpha hv)^2$-hv relation curve, E_g of TiO_2 NRAs is determined to 3.05 eV, which is in a good agreement with the previous reports[10,11].

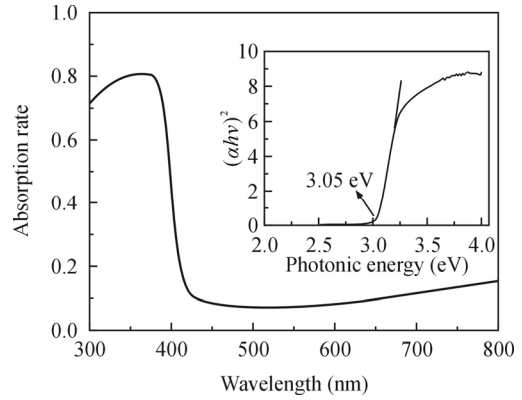

Fig.3 A typical optical transmittance spectrum of TiO_2 NRAs (The insert shows the corresponding $(\alpha hv)^2$-hv relation for determining the actual E_g.)

Fig.4(a) provides the LSV plots of TiO_2 NRAs measured under irradiation and in dark. The dark current density is rather low, while the photocurrent density increases rapidly from –0.385 V. That is to say, the onset potential is –0.385 V, which is also the open-circuit potential of TiO_2 NRAs. The saturate photocurrent density of 0.21 mA/cm^2 is obtained at 0.7 V. To evaluate the performance of TiO_2 NRAs, the applied bias photon-to-current efficiency (*ABPE*) is calculated by[12]

$$\eta = J \cdot (1.23 - V) / P , \quad (1)$$

where J is the current density under visible light irradiation, and V is the applied voltage versus reversible hydrogen electrode (RHE). Herein, the RHE potential can be deduced from the reference electrode of SCE by a relation as $E_{RHE}=E_{SCE}+0.24+0.059\cdot pH$. After calculation, the maximum *ABPE* is determined to be ~0.22%. Fig.4(b) indicates the amperometric *J-t* curve measured with light on/off cycles at a bias potential of 0 V versus SCE to examine the photocurrent response. A high on/off ratio of the current is observed, which indicates a good photosensitivity. Such a result is consistent with the LSV plots shown in Fig.4(a). Besides, a few spikes appear periodically in the *J-t* curve, which is possibly due to the carrier recombination. That phenomenon has been explained by the relatively poor charge separation ability in our previous studies[13]. Despite of those, it is also worth mentioning that the electrode remains a good stability even though undergoing a 200 min irradiation.

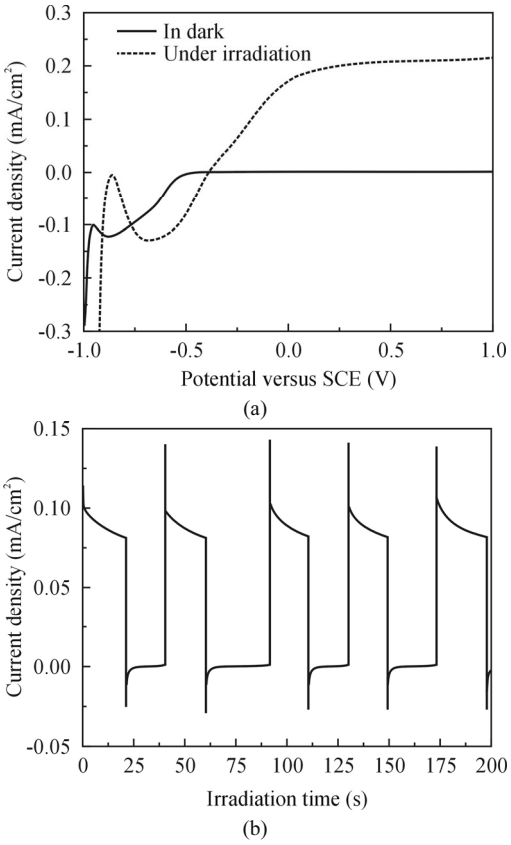

Fig.4 PEC measurement results: (a) LSV plots under irradiation and in dark; (b) Typical transient photocurrent response at 0.0 V bias (vs. SCE) of TiO_2 NRAs grown on FTO substrates under the simulated solar irradiation

Fig.5 displays the EIS results (Nyquist plots) recorded at open-circuit potential in dark and under irradiation. Two plots are well fitted by an equivalent circuit model shown in the inset of Fig.5, and the fitted data are indicated in Tab.1. In fact, it is clearly observed that the Nyquist plots are made up of two semicircles, corresponding to the resistance values of R_S and R_P, respectively. The smaller semicircle (R_S) of them over the high frequency range is related to the charge transferring process in the depletion layer (inside the nanorods), while the larger one should result from the electron transfer in the

Helmholtz layer (inside the electrolyte). As can be seen, both R_S and R_P are reduced when the light is turned on, suggesting that the charge transferring resistances are reduced a lot. That is to say, it is much easier for the electrons to enter the TiO_2 NRAs, which contributes to the increase of the current, namely, the photocurrent.

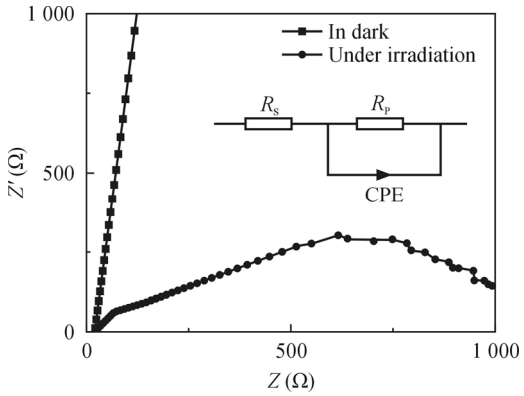

Fig.5 Results of electrochemical impedance measurements (the Nyquist plots) of TiO_2 NRAs under the irradiation and in dark (Inset shows an equivalent circuit used to fit the data.)

Tab.1 Fitted results from the Nyquist plots of TiO_2 NRA electrodes in dark and under irradiation through a facile equivalent circuit model shown in the inset of Fig.5

Condition	R_S (Ω)	R_P (Ω)	τ (s)
In dark	23	4.7×10^5	5.5×10^{-6}
Under irradiation	17	1.2×10^3	2.5×10^{-4}

Moreover, the M-S curves of TiO_2 NRAs are shown in Fig.6. It is a useful tool to analyze the doping density and the band bending in a semiconductor. Meanwhile, it is also known that the correlation between depletion layer capacitance (C) and applied potential (V) can be described by[14]

$$\frac{1}{C^2}=\frac{2}{e_0\varepsilon\varepsilon_0 N_d}\left[(V-V_{fb})-\frac{kT}{e_0}\right] , \quad (2)$$

where e_0 is the electron charge, ε is the dielectric constant, ε_0 is the permittivity of vacuum, N_d is the donor density for a n-type semiconductor, V is the applied potential, V_{fb} is the flat-band potential, and kT/e_0 is a temperature-dependent correction term. That is to say, the relation between $1/C^2$ and V remains linear around $V=V_{fb}$, meaning that the values of N_d and V_{fb} can be obtained easily by fitting the linear part of the curves. As shown in Tab.2, by fitting, N_d and V_{fb} are determined to be 2.3×10^{-18} cm^{-3} and –0.62 V in dark, which suggests that there is a background carrier density of 2.3×10^{-18} cm^{-3} inside nanorods and also a upward band bending of 0.62 V on the nanorod surface. It can be easily understood that V_{fb} refers to the potential at which no band bending occurs. In other words, a bias of –0.62 V is needed to reach a flat conduction band (CB) over the whole electrode region (including the surface and bulk).

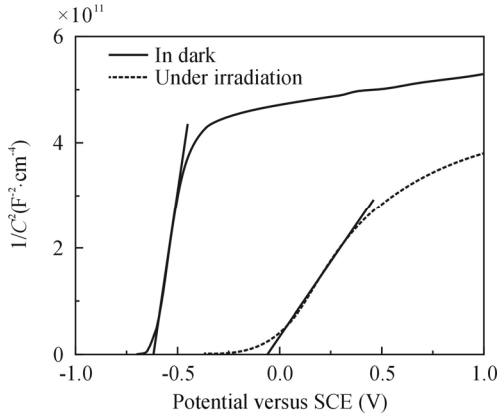

Fig.6 M-S curves of the TiO_2 NRA electrode at 0.0 V (versus SCE) in dark and under irradiation

Tab.2 Calculated parameters from M-S curves of TiO_2 NRA electrodes in dark and under irradiation

Condition	Slope k ($\times10^{11}$)	Flat band potential V_{fb} versus SCE (V)	Electron density N_D ($\times10^{18}$ cm^{-3})
In dark	26.8	−0.62	2.3
Under irradiation	5.9	−0.056	10.3

After initializing the irradiation, it is seen clearly that V_{fb} is shifted towards the positive side while N_d is increased by ~5 times. In order to explain the changes in M-S curves, a schematic mechanism is given in Fig.7. As we know, V_{fb} refers to a potential to compensate the band bending, and it corresponds to the potential of the Fermi level (E_F) at the undisturbed system[15]. It means that V_{fb} is actually close to the conduction band edge (CBE) of a n-type semiconductor like TiO_2. We know that the Fermi level is very close to the CBE of TiO_2 NRAs due to the presence of donor defects, like the oxygen vacancies (V_O). Naturally, a great number of electrons are generated and accumulated in the conduction band, owing to the effective transfer of the holes towards the electrolyte. As long as the irradiation is carried out continuously, the electron density remains a higher value inside the TiO_2 electrode than the case in dark, leading to a larger N_d measured by the M-S curves. In this paper, N_d is actually improved by nearly 5 times, which will result in an elevation of E_F value inevitably due to the well-known Burstein-Moss (B-M) effect[16]. As a result, V_{fd} is shifted toward the more positive side due to its close relationship with E_F. In addition, this behavior can also be understood that the conduction band is filled by more electrons, leading to the less band bending. It means that a lower potential is needed to reach the flat band of TiO_2 NRAs.

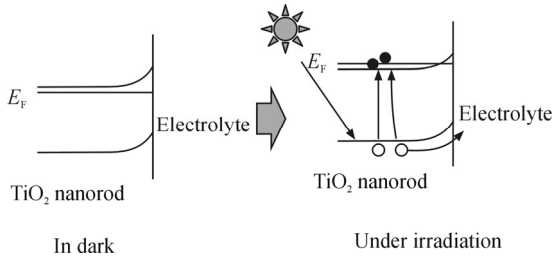

Fig.7 Schematic diagram of the energy levels of TiO_2 NRA electrodes in dark and under irradiation

In summary, TiO_2 NRAs were synthesized on FTO by a simple two-stage hydrothermal method. The nanorods exhibit a compact, oriented and single-crystal structure with a length of ~2 μm and a diameter of ~50 nm on the top. An *ABPE* of 0.22% is obtained for TiO_2 NRAs under a full-wavelength irradiation. Besides, we also compare the electrochemical results (including the Nyquist and M-S curves) of TiO_2 NRAs with and without the irradiation. We demonstrate that the irradiation enhances the charge transfer through the Helmholtz layer, resulting in the accumulation of electrons in the conduction band of TiO_2. As a result, compared with the data achieved in dark, N_d is increased, while V_{fb} is shifted towards the positive side. This work provides insight to better understand the PEC characteristics of a semiconductor, like TiO_2, ZnO or other materials.

References

[1] M. M. Momeni and Y. Ghaye, Journal of Electroanalytical Chemistry **751**, 43 (2015).

[2] X. C. Ni, L. X. Sang, H. J. Zhang, A. Kiliyanamkandy, S. Amoruso, X. Wang, R. Fittipaldi, T. Li, M. L. Hu and L. J. Xu, Optoelectronics Letters **10**, 43 (2014).

[3] B. O'Regan and M. Grätzel, Nature **353**, 737 (1991).

[4] J. R. Jenning, A. Ghicov, L. M. Peter, P. Schmuki and A. B. Walker, Journal of American Chemical Society **130**, 13364 (2008).

[5] B. L. Xu, C. X. Liu, H. Y. Sun and Y. R. Zhong, Optoelectronics Letters **10**, 84 (2014).

[6] S. A. Berhe, S. Nag, Z. Molinets and W. J. Youngblood, ACS Applied Materials & Interfaces **54**, 573 (2013).

[7] D. D. Qin, Y. P. Bi, X. J. Feng, W. Wang, G. D. Barber, T. Wang, Y. M. Song, X. Q. Lu and T. E. Mallouk, Chemistry of Materials **27**, 4180 (2015).

[8] M. Lv, D. Zheng, M. Ye, J. Xiao, W. Guo, Y. Lai, L. Sun, C. Lin and J. Zuo, , Energy & Environmental Science **6**, 1615 (2013).

[9] A. Yella, L. P. Heiniger, P. Gao, M. K. Nazeeruddin and M. Grätzel, Nano Letters **14**, 2591 (2014).

[10] A. Wolcott, W. A. Smith, T. R. Kuykendall, Y. Zhao and J. Z. Zhang, Small **5**, 104 (2009).

[11] X. Gu, S. Zhang, Y. Qiang, Y. Zhao and L. Zhu, Journal of Electronic Materials **43**, 2709 (2014).

[12] Z. Li, W. Luo, M. Zhang, J. Feng and Z. Zou, Energy & Environmental Science **6**, 347 (2013).

[13] M. Sui, C. Han, X. Gu, Y. Wang, L. Tang and H. Tang, Optoelectronics Letters **11**, 405 (2015).

[14] T. J. Jacobsson and T. Edvinsson, Journal of Physical Chemistry C **116**, 15692 (2012).

[15] H. P. Maruska and A. K. Ghosh, Solar Energy **20**, 443 (1978).

[16] E. Burstein, , Phys. Rev. B **93**, 632 (1954).